

Sisyphus Thermalization of Photons in a Double Quantum Dot

M. J. Gullans,^{1,2} J. Stehlik,³ Y.-Y. Liu,³ C. Eichler,³ J. R. Petta,³ and J. M. Taylor^{1,2}

¹*Joint Quantum Institute, National Institute of Standards and Technology, Gaithersburg, Maryland 20899, USA*

²*Joint Center for Quantum Information and Computer Science,
University of Maryland, College Park, Maryland 20742, USA*

³*Department of Physics, Princeton University, Princeton, New Jersey 08544, USA*

A strongly driven quantum system coupled to a thermalizing bath generically evolves into a highly non-thermal state as the external drive competes with the equilibrating force of the bath. We demonstrate a notable exception to this picture for a microwave resonator interacting with a periodically driven double quantum dot (DQD). In the limit of strong driving and long times, we show that the resonator field can be driven into a thermal state with a chemical potential given by a harmonic of the drive frequency. Such tunable chemical potentials are achievable with current devices and would have broad utility for quantum simulation in circuit quantum electrodynamics. As an example, we show how several DQDs embedded in an array of microwave resonators can induce a phase transition to a Bose-Einstein condensate of light.

When a physical system is subject to periodic driving, the usual notions of equilibrium thermodynamics have to be revisited. For a closed system, the second law of thermodynamics suggests it approaches an infinite temperature state; however, there are dramatic exceptions for integrable systems [1–7] and the recently discovered class of many-body localized phases [8–11]. For open systems, where the driven system is coupled to a fixed temperature bath, the system naturally reaches a steady state that evolves with the same periodicity as the drive; however, unlike in thermal equilibrium, no general classification scheme is believed to exist for such states [12]. Despite these challenges, many generic principles for these systems have been uncovered in recent years [12–17]

Solid-state quantum information systems are well suited to investigating these effects in a controlled setting [18–25]. The high degree of control and measurement capabilities enable arbitrary driving and accurate characterization of non-equilibrium states, while the host material acts as a large thermal bath to absorb the driving energy. In the case of electrical quantum dots and superconducting qubits, the typical frequencies of the qubits are low enough that it is relatively easy to enter a regime where the drive amplitude is much larger than the qubit frequency [22–26]. Furthermore, charge qubits in quantum dots have a very strong electron-phonon coupling, which, although detrimental for qubit operation, results in an efficient thermalization process [27, 28].

Here we consider a microwave resonator interacting with a periodically driven electron in a double quantum dot (DQD). The DQD is coupled to a fixed temperature phonon bath. In the limit of strong driving and long time, we show that the resonator field can approach a thermal state with a temperature given by the phonon temperature and a chemical potential given by a harmonic of the drive frequency. This system is an interesting case study for the emergence of thermal behavior in a periodically driven, open system. Furthermore, such tunable chemical potentials are achievable with current devices

and would have broad utility for quantum simulation in circuit quantum electrodynamics (cQED) [29–33].

We take the DQD to be configured near the charge transition between the states $|L\rangle$ and $|R\rangle$ with one electron (spin-less) in either the left or right dot, respectively. This pair of states has a large electric dipole moment that couples to the electric field in a nearby microwave resonator, as well as acoustic phonons in the semiconductor host [see Fig. 1(a)] [34–36].

We consider periodic driving of the level detuning $\epsilon(t) = \epsilon_0 + A \cos \omega t$, where ϵ_0 is an offset detuning and A and ω are the amplitude and frequency of the drive. In a process reminiscent of Sisyphus from Greek mythology, the DQD is continually excited by the drive, only to relax to the ground state via phonon and photon emission. For low driving amplitudes, $A \ll \hbar\omega$, the photon dynamics are dominated by resonance fluorescence of the DQD into the resonator [see Fig. 1(b)]. When $A \gtrsim \hbar\omega$, the situation changes dramatically because the two-level nature of the DQD leads to a series of sidebands at harmonics of the drive frequency up to $n_{\max} \approx A/\hbar\omega$ [37]. These sidebands give rise to a parametric “time-varying” coupling between resonator photons and phonons mediated by the DQD. Depending on the microscopic details, such parametric coupling of photons to a thermal bath can lead to a chemical potential for light [33].

To analyze the dynamics more closely, it is convenient to move into a Floquet basis where the time-dependent problem is mapped to a time-independent problem with an energy spectrum that is only well-defined modulo $\hbar\omega$ [38]. In the folded spectrum, the resonator frequency ω_c is mapped onto $\delta = \omega_c - n_c\omega$, where $n_c\omega$ is the closest harmonic to ω_c . The key insight is that near the resonances $\delta = 0$, the photon dynamics become dominated by Raman scattering events in which the DQD absorbs or emits a photon simultaneously with a phonon at frequency $|\delta|$. In a process we refer to as “Sisyphus thermalization,” these scattering events thermalize the resonator with these low energy phonons, giving rise to an effective

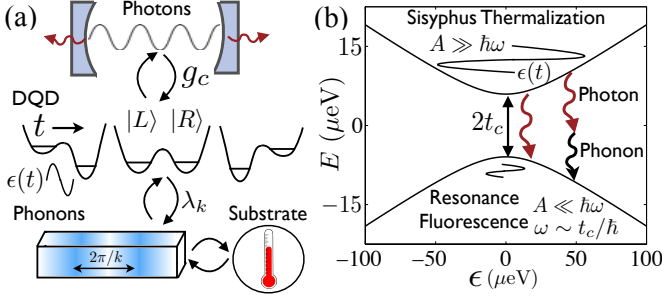


FIG. 1: (a) A microwave resonator is coupled to charge states in a DQD. The DQD is subject to periodic driving and strongly coupled to acoustic phonons, which are held at a fixed temperature. (b) Energy level diagram of the DQD with $t_c = 10 \mu\text{eV}$. For low drive amplitudes $A \ll \hbar\omega$, the photon dynamics are dominated by resonance fluorescence of the DQD into the resonator. At large amplitudes $A \gg \hbar\omega$, the phonon sideband dominates, leading to thermalization.

chemical potential for the photons $\mu = \hbar n_c \omega$.

Floquet Model – The Hamiltonian for the periodically driven DQD takes the form

$$H_c(t) = \frac{1}{2}(\epsilon_0 + A \cos \omega t)\sigma_z + t_c \sigma_x \quad (1)$$

where σ_ν are Pauli matrices operating in the $\{|L\rangle, |R\rangle\}$ orbital subspace, and t_c is the tunnel coupling between the dots. Including the resonator and phonons

$$H = H_c(t) + \hbar\omega_c a^\dagger a + \sum_k \hbar\omega_k a_k^\dagger a_k + \hat{X}\sigma_z, \quad (2)$$

where ω_k is the frequency of the k th phonon mode, $a(a^\dagger)$ and $a_k(a_k^\dagger)$ are the bosonic photon and phonon annihilation(creation) operators, respectively, $\hat{X}/\hbar = g_c(a + a^\dagger) + \sum_k \lambda_k(a_k^\dagger + a_k)$ contains the coupling g_c between the resonator and DQD, as well as the coupling λ_k between the DQD and the phonons.

From Floquet theory [37, 38], we know that the evolution under such time-periodic Hamiltonians can be formally represented using an infinite dimensional basis $|m\rangle$ for integers m . In this representation, $H(t)$ is mapped to a time-independent Hamiltonian H_F by adding the term $\hbar\omega\hat{N} = \sum_m \hbar\omega m|m\rangle\langle m|$ and converting the functions $e^{-im\omega t}$ into operators which change the Floquet index by m , i.e., $\hat{F}_m = \sum_{m'} |m+m'\rangle\langle m'|$.

Before writing H_F , we apply three unitary transformations that map the problem to a convenient basis. First, we apply a polaron transformation that dresses the DQD with the ambient phonons and photons in the environment [39, 40]

$$U_p = e^{[g_c(a - a^\dagger)/\omega_c + \sum_k \lambda_k(a_k - a_k^\dagger)/\omega_k] \sigma_z}. \quad (3)$$

The transformation $U_p H U_p^\dagger$ removes the $\hat{X}\sigma_z$ term and results in explicit interaction terms between photons and

phonons. These terms were previously identified as giving rise to a strong phonon sideband in the emission spectrum of the DQD [40]. As illustrated in Fig. 1(b), in the context of the present work, they lead to efficient equilibration between the resonator and the phonons. The second transformation, motivated by the strong periodic driving, folds the resonator and phonon spectrum into a band between $\pm\omega/2$

$$U_{RW}(t) = e^{-in_c \omega a^\dagger t} \prod_{n \geq 0} \prod_{k \in \Omega_n} e^{-in\omega a_k^\dagger a_k t} \quad (4)$$

where Ω_n is the set of k such that $(n-1/2)\omega < \omega_k < (n+1/2)\omega$. Finally, we apply a unitary U_F (found numerically) such that $U_F H_c U_F^\dagger$ is diagonal. This modifies the coupling between the DQD and the photons and phonons, which we account for by introducing the tensor $u_{\nu n}^{\mu m}$ such that

$$U_F \sigma_\nu \hat{F}_n U_F^\dagger = \sum_{\mu \in \{x, y, z\}} \sum_{m=-\infty}^{\infty} u_{\nu n}^{\mu m} \sigma_\mu \hat{F}_m \quad (5)$$

With these transformations the Floquet Hamiltonian, to lowest order in g_c/ω_c and λ_k/ω_k , is

$$\frac{H_F}{\hbar} = \frac{\Delta}{2} \sigma_z + \delta a^\dagger a + \sum_{n, k \in \Omega_n} (\omega_k - n\omega) a_k^\dagger a_k + \omega \hat{N} \quad (6)$$

$$+ (\hat{V}_{cp} + \hat{V}_{cpp} + h.c.)$$

$$\hat{V}_{cp} = \sum_{n, \mu, m} u_{\nu n}^{\mu m} \left(\frac{2it_c g_c}{\hbar\omega_c} \delta_{nn_c} a + \hat{R}_n \right) \sigma_\mu \hat{F}_m \quad (7)$$

$$\hat{V}_{cpp} = \sum_{n, \mu, m} \frac{g_c \hat{R}_n}{\omega_c} (u_{xn+nc}^{\mu m} a + u_{xn-nc}^{\mu m} a^\dagger) \sigma_\mu \hat{F}_m \quad (8)$$

where $\pm \hbar\Delta/2$ are the two quasi-energies of H_c^F , $\hat{R}_n = \sum_{k \in \Omega_n} \frac{2it_c \lambda_k}{\hbar\omega_k} a_k$, and the summation limits are the same as above.

Steady State – To determine the effect of the driven DQD on the resonator field, we first find the steady state dynamics with $g_c = 0$. When $t_c g_c / \hbar\omega_c \ll \Delta$, we can use this solution to determine the resonator field because it has negligible back-action on the DQD [41]. To a good approximation, each Floquet block evolves independently from the others because H_F has the property that single phonon processes only resonantly couple states with the same Floquet index. Using a generalization of Fermi's Golden rule for Floquet systems [13], the rate to spontaneously emit a phonon in the Ω_n band with $n \geq 0$ and make a transition from the upper(lower) to the lower(upper) state is

$$\gamma_{n\mp} = \frac{8\pi t_c^2 / \hbar^2}{(n\omega \pm \Delta)^2} (|u_{ym}^{x0}|^2 + |u_{yn}^{y0}|^2) J(n\omega \pm \Delta). \quad (9)$$

where $J(\nu) = \sum_k |\lambda_k|^2 \delta(\nu - \omega_k)$ is the phonon spectral density. We assume the phonons are in thermal equilibrium with temperature T and distributed according

to the Bose function $n_p(\nu) = (e^{\hbar\nu/k_B T} - 1)^{-1}$. In this case, there is also stimulated emission and absorption at the rates $\gamma_{n\mp}^s = \gamma_{n\mp} n_p(n\omega \pm \Delta)$. Introducing the total transition rate from the upper(lower) to the lower(upper) DQD states $\gamma_{\mp} = \sum_n \gamma_{n\mp} + \gamma_{n\mp}^s + \gamma_{n\mp}^s$, the effective master equation for the DQD within each Floquet block is

$$\dot{\rho}_n = i\frac{\Delta}{2}[\sigma_z, \rho_n] + \gamma_- \mathcal{D}[\sigma_-]\rho_n + \gamma_+ \mathcal{D}[\sigma_+]\rho_n, \quad (10)$$

where $\mathcal{D}[c]\rho_n = -1/2\{c^\dagger c, \rho_n\} + c\rho_n c^\dagger$ and the total density matrix for the DQD is $\rho_d = \sum_n \rho_n |n\rangle\langle n|$. This master equation can be used to derive the steady state and all time-dependent correlation functions of the DQD [42].

Chemical Potential for Light – Based on the discussions above, for finite g_c , we expect three possible types of output light. When resonance fluorescence dominates, the DQD acts as a single photon source and produces anti-bunched light. When $\langle\sigma_\nu\rangle \neq 0$ for some ν , we see from Eq. (7) that the DQD will drive the resonator into a coherent state; alternatively, when there is a large amount of gain, the system can begin lasing and produce a coherent state [43]. Finally, if the DQD mostly acts to thermalize the resonator, the light will exhibit thermal statistics.

Conveniently, the four-point correlation function

$$g^{(2)}(0) = \lim_{t \rightarrow \infty} \frac{\langle a^\dagger(t) a^\dagger(t) a(t) a(t) \rangle}{\langle a^\dagger(t) a(t) \rangle^2} \quad (11)$$

can distinguish these three states because for anti-bunched light $g^{(2)}(0) = 0$, for a coherent state $g^{(2)}(0) = 1$, and for thermal light $g^{(2)}(0) = 2$. Figure 2(a) shows $g^{(2)}(0)$ for a nanowire DQD, calculated following the approach detailed in the supplementary material [42], over a large range of A and ω . We set $J(\nu)$ by noting that it is proportional to a dimensionless function of ν , which we found by assuming a 25 nm radius nanowire with a separation between the two dots of 120 nm, an axial confinement of 25 nm for each dot, and a phonon speed of sound of 4000 m/s [39]. We set the proportionality constant by fixing the DQD relaxation rate at zero detuning to be 6 ns^{-1} [28, 44]. Other parameters were taken from recently measured values in InAs nanowire DQDs [45].

Although the behavior of $g^{(2)}(0)$ shown in Fig. 2(a) is a complex function of the drive parameters, there are large regions where the light has mostly thermal correlations. These thermal regions occur when ω becomes resonant with a sub-harmonic of ω_c . Away from these resonances, the light is either strongly anti-bunched or a mixture of thermal, anti-bunched, and coherent light.

We focus on the thermal regions in the present work. To better understand how they emerge note that, near these resonances, the photon dynamics are dominated by incoherent scattering processes in which both a photon and phonon are absorbed or emitted without changing the state of the DQD [see inset of Fig. 2(b)]. This occurs

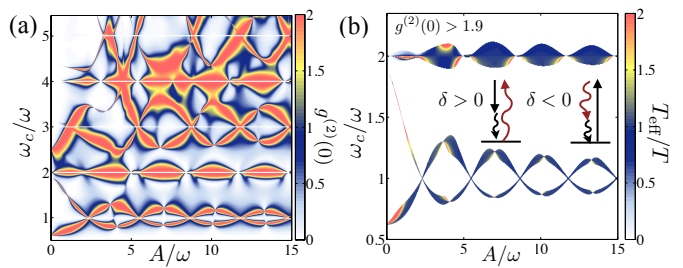


FIG. 2: (a) Four-point correlation function $g^{(2)}(0)$ in the strong driving limit. We took $\omega_c/2\pi = 16 \text{ GHz}$, $t_c = 20 \text{ } \mu\text{eV}$, $\epsilon_0 = 0$, $g_c/2\pi = 30 \text{ MHz}$, $\kappa/2\pi = 2.6 \text{ MHz}$, and $T = 100 \text{ mK}$. The regions close to the resonances $\omega_c/\omega = n_c$ are excluded. (b) Effective temperature from Eq. (15) for the same parameters as (a). Only shown in the regions where $g^{(2)}(0) > 1.9$. (Inset) Raman scattering processes when $\delta = \omega_c - n_c\omega$ is near zero. The red line is a photon, the solid line is the drive, and the curved black line is a phonon.

because the spectral density for these Raman processes

$$J_R(\delta) = \sum_k \frac{4t_c^2 g_c^2 |\lambda_k|^2}{\hbar^2 \omega_k^2 \omega_c^2} \delta(\delta - \omega_k) = \frac{4t_c^2 g_c^2}{\hbar^2 \omega_c^2} \frac{J(\delta)}{\delta^2} \quad (12)$$

diverges near these resonances when $J(\nu)$ decays to zero more slowly than ν^2 (e.g., as in the case of piezoelectric coupling in a nanowire DQD where $J(\nu) \sim \nu$ [44]). As a result, the photons follow a simple master equation

$$\dot{\rho}_c = i\delta[a^\dagger a, \rho_c] + (\kappa + R_a)\mathcal{D}[a]\rho_c + R_e \mathcal{D}[a^\dagger]\rho_c \quad (13)$$

where κ is the resonator decay rate and $R_{a(e)}$ are the phonon-assisted, photon absorption(emission) rates, respectively. When $R_e \neq 0$ and $R_e < \kappa + R_a$, this master equation always leads to a thermal distribution with $g^{(2)}(0) = 2$ [46].

To see how the chemical potential emerges, we have to consider the regimes $\omega < \omega_c/n_c$ and $\omega > \omega_c/n_c$ separately. When $\omega < \omega_c/n_c$ the dominant processes are ones in which a photon is emitted(absorbed) along with the absorption(emission) of a phonon with frequency $\delta = \omega_c - n_c\omega$. In this case, $R_e \approx R n_p(\delta)$ and $R_a \approx R [n_p(\delta) + 1]$. From Eq. (8) and Fermi's Golden rule for Floquet systems, we can calculate [42]

$$R = 2\pi |u_{xn_c}^z|^2 J_R(\delta). \quad (14)$$

When $\omega > \omega_c/n_c$, a photon is emitted or absorbed simultaneously with a phonon at frequency $-\delta > 0$. In this case, photon emission and absorption are reversed and $R_e = R [n_p(-\delta) + 1]$ and $R_a = R n_p(-\delta)$. As δ approaches zero from this side of the resonance, the gain rate of the resonator $R_e - R_a = R$ diverges and, at some point, will exceed κ . At this point, the system begins lasing and many of our approximations in deriving $g^{(2)}(0)$ break down. A full analysis of the saturation mechanisms

for this type of laser (including non-Markovian effects in the phonon bath) is beyond the scope of the present work. As a result, these regions are excluded from our calculation of $g^{(2)}(0)$ in Fig. 2(a). Despite this instability, the resonator field will still satisfy detailed balance until saturation effects take hold and, on both sides of the resonance, we can define an effective temperature through the relation

$$\frac{R_e}{R_a} = e^{-\hbar(\omega_c - n_c\omega)/k_B T_{\text{eff}}}. \quad (15)$$

Our analysis above predicts $T_{\text{eff}}/T = 1$ in these thermal regions. Figure 2(b) shows T_{eff}/T in the regions where $g^{(2)}(0) > 1.9$, including many additional photon emission(absorption) processes in $R_{e(a)}$ [42]. We see that this ratio is indeed close to one over a large range of A and ω . These are the main results of this work and indicate that, for small δ , the identification of $\hbar n_c \omega$ with a chemical potential is well justified, while, for large δ , the DQD can act as a single photon source.

BEC of Light – When the resonators are arranged in a large array, the low energy spectrum generically has the dispersion of a massive particle $\varepsilon_{\mathbf{k}} = \hbar\omega_c + \hbar^2 |\mathbf{k}|^2 / 2m$, where \mathbf{k} is the quasi-momentum and m is the effective mass. When such “massive” photons equilibrate at low temperatures, they can form a Bose-Einstein condensate (BEC) [47, 48]. One of the defining features of a BEC is a macroscopic occupation of the $\mathbf{k} = 0$ mode in the thermodynamic limit, which can be inferred by measuring a finite condensate fraction

$$f = \frac{n_0}{n_0 + \sum_{|\mathbf{k}|>0} n_{\mathbf{k}}}, \quad (16)$$

where $n_{\mathbf{k}}$ is the mean photon number in mode \mathbf{k} .

As an illustrative example of how the chemical potential for photons described here produces a BEC, we consider a square lattice of resonators in one (1D), two (2D), and three (3D) dimensions [see Fig. 3(a)]. The effective mass is $m = \hbar/2a^2t$, where a is the lattice spacing and t is the nearest-neighbor hopping rate. The Hamiltonian for the resonator photons interacting with a dilute ensemble of DQDs is

$$H = \sum_{\mathbf{k}} \varepsilon_{\mathbf{k}} a_{\mathbf{k}}^\dagger a_{\mathbf{k}} + \sum_{i=1}^{N_d} [H_c^i(t) + \sum_q \hbar\omega_q b_{iq}^\dagger b_{iq} + \hat{X}_i \sigma_z^i],$$

$$\frac{\hat{X}_i}{\hbar} = \sum_{\mathbf{k}} \frac{g_c e^{i\mathbf{k}\cdot\mathbf{r}_i}}{\sqrt{N}} (a_{\mathbf{k}} + a_{\mathbf{k}}^\dagger) + \sum_q \lambda_q (b_{iq} + b_{iq}^\dagger),$$

where $a_{\mathbf{k}}$ are the bosonic operators for the resonator array, b_{iq} are the bosonic operators for the phonons coupled to the i th DQD at position \mathbf{r}_i , σ_z^i are local Pauli operators, and $N(N_d)$ is the number of resonators(DQDs). For a DQD driven at a frequency ω near ω_c/n_c , the analysis in the previous section implies

$$n_{\mathbf{k}} = \frac{n_d R_e(\delta_{\mathbf{k}})}{n_d [R_a(\delta_{\mathbf{k}}) - R_e(\delta_{\mathbf{k}})] + \kappa} = \frac{n_p(\delta_{\mathbf{k}})}{1 + \frac{\kappa}{n_d R(\delta_{\mathbf{k}})}}, \quad (17)$$

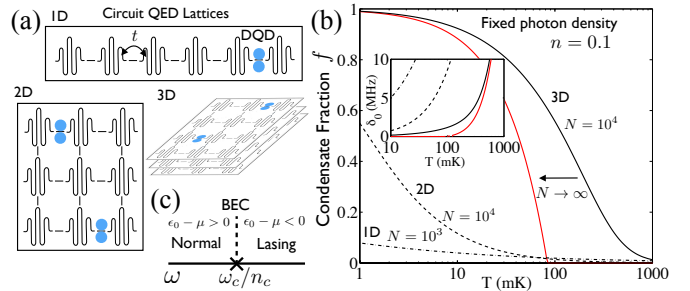


FIG. 3: (a) Circuit QED lattices for creation of BEC. The nearest neighbor hopping rate is t and a small fraction n_d of the resonators are coupled to a DQD. (b) Condensate fraction as a function of temperature with (inset) δ_0 chosen such that $n = 0.1$. For 1D and 2D there is no BEC as $N \rightarrow \infty$, but a large condensate fraction can be sustained at finite N . In 3D there is a phase transition to a BEC at $T_c \approx 100$ mK. We took parameters as in Fig. 2 with $t/2\pi = 100$ MHz, $n_d = 1\%$, $n_c = 2$, $u_{x n_c}^z = 1/2$, and $\kappa/2\pi = 1$ MHz. (c) Phase diagram as a function of drive frequency ω . When $\omega = \omega_c/n_c$, the system can form a BEC in the thermodynamic limit, above this value a finite fraction of the modes begin lasing.

where $\hbar\delta_{\mathbf{k}} = \varepsilon_{\mathbf{k}} - \mu$, $\mu = \hbar n_c \omega$ is the effective chemical potential, and $n_d = N_d/N$ is the fraction of resonator sites coupled to a DQD.

In equilibrium, it is well known that a finite temperature BEC only exists for such a uniform system in dimension $d > 2$ [49]. Figure 3(b) shows f calculated for experimentally relevant parameters for finite N [42]. For each temperature, we chose the effective chemical potential to fix the photon density $n = (n_0 + \sum_{|\mathbf{k}|>0} n_{\mathbf{k}})/N = 0.1$ [see inset to Fig. 3(b)]. A large condensate fraction can be sustained at finite N in 1D and 2D; however, f stays finite in the thermodynamic limit only in 3D [42]. The critical temperature at this density is $T_c \approx 100$ mK. Recently, 2D arrays with as many as 200 sites have been realized [31]. Arrays with dimension $d > 2$ can be achieved by stacking 2D arrays, as illustrated in Fig. 3(a), or through engineered long range hopping in 2D [50].

This discussion focused on the regime $\omega \leq \omega_c/n_c$. For $\omega > \omega_c/n_c$, a finite fraction of the modes have gain greater than loss and can start lasing [see Fig. 3(b)]. This regime is analogous to photon condensates in dye filled microcavities [47] and polariton condensates in exciton-polariton systems [48] and is a rich avenue for further investigation.

Conclusions – We have demonstrated that a strongly driven DQD can induce thermalization of photons in a nearby microwave resonator into a state with an effective chemical potential. The emergence of thermal behavior in a strongly driven, dissipative system is an interesting counter-example to the generic behavior of such systems. Moreover, we have shown these effects are readily achievable in current devices based on InAs nanowire

DQDs. This suggests a novel application of these devices for quantum simulation in cQED lattices. For example, a practical improvement over Ref. [33] is the realization of a chemical potential for light at a harmonic of the drive frequency, which enables efficient rejection of the drive field. More generally, though, this work shows that strong coupling to a thermal bath, which is naturally provided by DQDs, is a valuable resource for cQED systems.

Acknowledgements – This research was supported in part by the National Science Foundation under Grant No. NSF PHY11-25915, NIST, and the NSF Physics Frontier at the JQI. Research at Princeton was supported by the Gordon and Betty Moore Foundation’s EPiQS Initiative through Grant No. GBMF4535, with partial support from the Packard Foundation and the National Science Foundation (Grants No. DMR-1409556 and DMR-1420541).

-
- [1] P. L. Kapitza, Soviet Phys. JETP **21**, 588 (1951).
 [2] M. A. Lieberman, A. J. Lichtenberg, Phys. Rev. A **5**, 1852 (1972).
 [3] G. Casati and J. Ford, *Stochastic Behavior in Classical and Quantum Hamiltonian Systems*, vol. 93, (Springer, Berlin, Heidelberg, 1979).
 [4] D. R. Grempel, R. E. Prange, and S. Fishman, Phys. Rev. A **29**, 1639 (1984).
 [5] R. Graham, M. Schlautmann, and P. Zoller, Phys. Rev. A **45**, R19 (1992).
 [6] F. L. Moore, J. C. Robinson, C. Bharucha, P. E. Williams, and M. G. Raizen, Phys. Rev. Lett. **73**, 2974 (1994).
 [7] G. Lemarié, J. Chabé, P. Szriftgiser, J. C. Garreau, B. Grémaud, and D. Delande, Phys. Rev. A **80**, 043626 (2009).
 [8] D. M. Basko, I. L. Aleiner, and B. L. Altshuler, Ann. Phys. **321**, 1126 (2006).
 [9] A. Pal, D. A. Huse, Phys. Rev. B **82** 174411 (2010).
 [10] L. D’Alessio and A. Polkovnikov, Ann. Phys. **333**, 19 (2013).
 [11] P. Ponte, A. Chandran, Z. Papić, and D. A. Abanin, Ann. Phys. **353**, 196 (2015).
 [12] W. Kohn, J. Stat. Phys. **103**, 417 (2001).
 [13] T. Kitagawa, T. Oka, A. Brataas, L. Fu, and E. Demler, Phys. Rev. B **84**, 235108 (2011).
 [14] N. H. Lindner, G. Refael, and V. Galitski, Nature Phys. **7**, 490 (2011).
 [15] Y. H. Wang, H. Steinberg, P. Jarillo-Herrero, and N. Gedik, Science **342**, 453 (2013).
 [16] M. Langemeyer and M. Holthaus, Phys. Rev. E **89**, 012101 (2014).
 [17] T. Shirai, T. Mori, and S. Miyashita, Phys. Rev. E **91**, 030101 (2015).
 [18] W. D. Oliver, Y. Yu, J. C. Lee, K. K. Berggren, L. S. Levitov, and T. P. Orlando, Science **310**, 1653 (2005).
 [19] M. Sillanpää, T. Lehtinen, A. Paila, Y. Makhlin, and P. Hakonen, Phys. Rev. Lett. **96**, 187002 (2006).
 [20] L. Childress and J. McIntyre, Phys. Rev. A **82**, 033839 (2010).
 [21] G. D. Fuchs, G. Burkard, P. V. Klimov, and D. D. Awschalom, Nature Phys. **7**, 789 (2011).
 [22] S. Shevchenko, S. Ashhab, and F. Nori, Phys. Rep. **492**, 1 (2010).
 [23] J. R. Petta, H. Lu, and A. C. Gossard, Science **327**, 669 (2010).
 [24] L. Gaudreau, G. Granger, A. Kam, G. C. Aers, S. A. Studenikin, P. Zawadzki, M. Pioro-Ladrière, Z. R. Wasilewski, and A. S. Sachrajda, Nature Phys. **8**, 54 (2012).
 [25] J. Stehlik, Y. Dovzhenko, J. R. Petta, J. R. Johansson, F. Nori, H. Lü, and A. C. Gossard, Phys. Rev. B **86**, 121303 (2012).
 [26] C. Deng, J.-L. Orgiazzi, F. Shen, S. Ashhab, and A. Lupascu, Phys. Rev. Lett. **115**, 133601 (2015).
 [27] T. Fujisawa, T. H. Oosterkamp, W. G. van der Wiel, B. W. Broer, R. Aguado, S. Tarucha, and L. P. Kouwenhoven, Science **282**, 932 (1998).
 [28] J. R. Petta, A. C. Johnson, C. M. Marcus, M. P. Hanson, and A. C. Gossard, Phys. Rev. Lett. **93**, 186802 (2004).
 [29] M. J. Hartmann, F. G. S. L. Brandao, and M. B. Plenio, Nature Phys. **2**, 849 (2006).
 [30] A. D. Greentree, C. Tahan, J. H. Cole, L. C. L. Hollenberg, Nature Phys. **2**, 856 (2006).
 [31] A. A. Houck, H. E. Türeci, and J. Koch, Nature Phys. **8**, 292 (2012).
 [32] M. Schiró, M. Bordyuh, B. Öztöp, and H. E. Türeci, Phys. Rev. Lett. **109**, 053601 (2012).
 [33] M. Hafezi, P. Adhikari, and J. M. Taylor, arXiv:1405.5821 (2014).
 [34] L. Childress, A. S. Sorensen, and M. D. Lukin, Phys. Rev. A **69**, 042302 (2004).
 [35] K. D. Petersson, L. W. McFaul, M. D. Schroer, M. Jung, J. M. Taylor, A. A. Houck, and J. R. Petta, Nature (London) **490**, 380 (2012).
 [36] T. Frey, P. J. Leek, M. Beck, A. Blais, T. Ihn, K. Ensslin, and A. Wallraff, Phys. Rev. Lett. **108**, 046807 (2012).
 [37] M. Grifoni and P. Hänggi, Phys. Rep. **304**, 229 (1998).
 [38] H. Sambe, Phys. Rev. A **7**, 2203 (1973).
 [39] T. Brandes, Phys. Rep. **408**, 315 (2005).
 [40] M. J. Gullans, Y.-Y. Liu, J. Stehlik, J. R. Petta, and J. M. Taylor, Phys. Rev. Lett. **114**, 196802 (2015).
 [41] This assumption breaks down at large intracavity photon numbers (e.g., during lasing).
 [42] See supplemental material for an outline of the derivation of $g^{(2)}(0)$ and $R_{e(a)}$ and more BEC data at finite N .
 [43] Y. Y. Liu, J. Stehlik, C. Eichler, M. J. Gullans, J. M. Taylor, and J. R. Petta, Science **347**, 285 (2015).
 [44] C. Weber, A. Fuhrer, C. Fasth, G. Lindwall, L. Samuelson, and A. Wacker, Phys. Rev. Lett. **104**, 036801 (2010).
 [45] Y.-Y. Liu, K. D. Petersson, J. Stehlik, J. M. Taylor, and J. R. Petta, Phys. Rev. Lett. **113**, 036801 (2014).
 [46] M. O. Scully and S. Zubairy, *Quantum Optics* (Cambridge University Press, 1997).
 [47] J. Klaers, J. Schmitt, F. Vewinger, and M. Weitz, Nature (London) **468**, 545 (2010).
 [48] T. Byrnes, N. Y. Kim, and Y. Yamamoto, Nature Phys. **10**, 803 (2014).
 [49] F. Dalfovo, S. Giorgini, L. P. Pitaevskii, and S. Stringari, Rev. Mod. Phys. **71**, 463 (1999).
 [50] D. I. Tsomokos, S. Ashhab, and F. Nori, Phys. Rev. A **82**, 052311 (2010).

Supplemental Material

Photon Correlation Functions – The master equation for the DQD with $g_c = 0$ [Eq. (12) in the main text] can be used to evaluate all correlation functions of the form $\langle \prod_{i=1}^n \sigma_{\nu_i}(t_i) \rangle$ using the quantum regression theorem [46]. In particular, the Liouvillian associated with this master equation can be written as a matrix operating on the vector of the density matrix components $\rho_n = (\rho_n^{--}, \rho_n^{-+}, \rho_n^{+-}, \rho_n^{++})^T$ as

$$\mathcal{L} = \begin{pmatrix} -\gamma_+ & 0 & 0 & \gamma_- \\ 0 & -(\gamma - i\Delta) & 0 & 0 \\ 0 & 0 & -(\gamma + i\Delta) & 0 \\ \gamma_+ & 0 & 0 & -\gamma_- \end{pmatrix} \quad (\text{S1})$$

where $\gamma = (\gamma_+ + \gamma_-)/2$ is the dephasing rate. The steady state is

$$\rho_{ss} = \left(\frac{\gamma_+}{2\gamma}, 0, 0, \frac{\gamma_-}{2\gamma} \right)^T \quad (\text{S2})$$

A complete basis of operators acting on the two-level system is given by $\hat{\Lambda}_{\pm} = \sigma_{\pm}$ and $\hat{\Lambda}_z = \sigma_z - \langle \sigma_z \rangle$, which

have the simple time evolution under \mathcal{L}

$$\langle \hat{\Lambda}_{\pm}(t) \rangle = \langle \hat{\Lambda}_{\pm}(0) \rangle e^{-(\gamma \pm i\Delta)t}, \quad (\text{S3})$$

$$\langle \hat{\Lambda}_z(t) \rangle = \langle \hat{\Lambda}_z(0) \rangle e^{-2\gamma t}. \quad (\text{S4})$$

We let τ be the permutation such that $t_{\tau(1)} > t_{\tau(2)} > \dots > t_{\tau(n)}$, then Eq. (S3) and Eq. (S4) imply

$$\langle \prod_i \hat{\Lambda}_{\nu_i}(t_i) \rangle = f_{\nu_1, \dots, \nu_n}(t_1, \dots, t_n) \langle \prod_i \hat{\Lambda}_{\nu_i}(0) \rangle, \quad (\text{S5})$$

$$f_{\nu_1, \dots, \nu_n}(t_1, \dots, t_n) = \prod_{i=1}^{n-1} e^{-\gamma_{\nu_{\tau(i)}} [t_{\tau(i)} - t_{\tau(i+1)}]}, \quad (\text{S6})$$

where $\gamma_{\pm} = \gamma \pm i\Delta$ and $\gamma_z = 2\gamma$.

To find the correlation functions for the cavity field we treat the phonons as a Markovian bath and derive the Heisenberg-Langevin equations of motion for a [46]

$$\dot{a} = -\left(\frac{\kappa + \hat{R}_a - \hat{R}_e}{2} + i\delta \right) a + \sum_{m,\nu} \frac{2it_c g_c}{\hbar\omega_c} u_{y_n c}^{\nu m} \hat{\Lambda}_{\nu} \hat{F}_m + \sum_m \frac{2it_c g_c}{\hbar\omega_c} u_{y_n c}^{zm} \langle \sigma_z \rangle \hat{F}_m + \sum_{\nu} \sigma_{\nu} (\hat{\mathcal{F}}_{a\nu} + \hat{\mathcal{F}}_{e\nu}^{\dagger}) + \hat{\mathcal{F}}_c, \quad (\text{S7})$$

$$\hat{R}_a = \sum_{n \geq 0} \gamma_{az}^n + \gamma_{a+}^n (1 - \sigma_z)/2 + \gamma_{a-}^n (1 + \sigma_z)/2, \quad (\text{S8})$$

$$\hat{R}_e = \sum_{n \geq 0} \gamma_{ez}^n + \gamma_{e+}^n (1 - \sigma_z)/2 + \gamma_{e-}^n (1 + \sigma_z)/2 \quad (\text{S9})$$

Each term in $\hat{R}_{e(a)}$ arises from the corresponding phonon-assisted, photon emission(absorption) processes labeled in Fig. (S1). They can be derived from Fermi's Golden rule for Floquet states as

$$\gamma_{az}^n = |u_{xn-n_c}^{z0}|^2 J_R(\delta + n\omega), \quad (\text{S10})$$

$$\gamma_{ez}^n = |u_{xn+n_c}^{z0}|^2 J_R(-\delta + n\omega), \quad (\text{S11})$$

$$\gamma_{a\pm}^n = |u_{xn-n_c}^{\pm m_{a\pm}}|^2 J_R[\delta \pm \Delta + (n + m_{a\pm})\omega], \quad (\text{S12})$$

$$\gamma_{e\pm}^n = |u_{xn+n_c}^{\pm m_{e\pm}}|^2 J_R[-\delta \pm \Delta + (n + m_{e\pm})\omega], \quad (\text{S13})$$

where J_R is defined in Eq. (14) of the main text, $m_{e\pm}$ is the closest integer to $(\delta \mp \Delta)/\omega$, and $m_{a\pm}$ is the closest integer to $(-\delta \mp \Delta)/\omega$. They each have an associated noise operator $\hat{\mathcal{F}}_{e(a)\nu}$ which satisfy

$$\langle \hat{\mathcal{F}}_{az}^{\dagger}(t) \hat{\mathcal{F}}_{az}(t') \rangle = \sum_{n \geq 0} \gamma_{az}^n n_p(\delta + n\omega) \delta(t - t'), \quad (\text{S14})$$

$$[\hat{\mathcal{F}}_{az}(t), \hat{\mathcal{F}}_{az}^{\dagger}(t')] = \sum_{n \geq 0} \gamma_{az}^n \delta(t - t'), \quad (\text{S15})$$

and similarly for the other noise operators. $\hat{\mathcal{F}}_c$ is the noise operator associated with the cavity decay κ and satisfies

$$\langle \hat{\mathcal{F}}_c^{\dagger}(t) \hat{\mathcal{F}}_c(t') \rangle = \kappa n_p(\omega_c) \delta(t - t'), \quad (\text{S16})$$

$$[\hat{\mathcal{F}}_c(t), \hat{\mathcal{F}}_c^{\dagger}(t')] = \kappa \delta(t - t') \quad (\text{S17})$$

To calculate the correlation functions of a we first approximate $\hat{R}_{e(a)}$ by their expectation values and formally integrate the equation for a

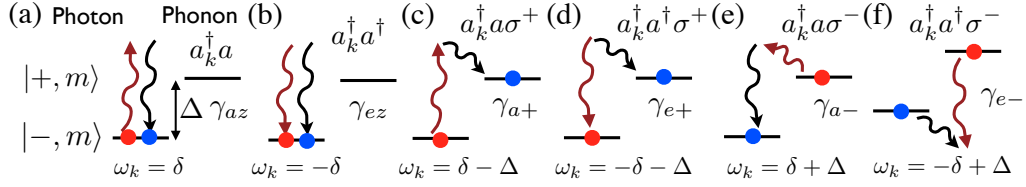


FIG. S1: (a-f) Various phonon-assisted-photon processes starting from the state with the red circle and ending in the state with the blue circle.

$$\begin{aligned}
 a(t) = & \sum_m \frac{2it_c g_c}{\hbar \omega_c} \frac{u_{y m_c}^{z m} \langle \sigma_z \rangle \hat{F}_m(t)}{(\kappa + R_a - R_e)/2 + i(\delta + m\omega)} + \sum_m \frac{2it_c g_c}{\hbar \omega_c} u_{y m_c}^{\nu m} \hat{F}_m(t) \int_{-\infty}^t dt' e^{-[(\kappa + R_a - R_e)/2 + i\delta](t-t')} \hat{\Lambda}_\nu(t') e^{im\omega t'} \\
 & + \int_{-\infty}^t dt' e^{-[(\kappa + R_a - R_e)/2 + i\delta](t-t')} \left\{ \sum_\nu \sigma_\nu(t') [\hat{\mathcal{F}}_{a\nu}(t') + \hat{\mathcal{F}}_{e\nu}^\dagger(t')] + \hat{\mathcal{F}}_c(t') \right\}. \quad (\text{S18})
 \end{aligned}$$

This analysis shows that the resonator field has three distinct contributions. The first term describes coherent light arising from the strong driving of the DQD, the second term arises from the resonance fluorescence of the DQD and gives rise to anti-bunched light, and the third term describes the thermal contributions to the light (note this analysis breaks down when the system starts lasing). From Eq. (S18) and Eq. (S5), we can derive an expression for $g^{(2)}(0)$

$$g^{(2)}(0) = \frac{2(\langle a^\dagger a \rangle^2 - \langle a^\dagger a \rangle_0^2) + \langle a^\dagger a^\dagger a a \rangle_0}{\langle a^\dagger a \rangle^2} \quad (\text{S19})$$

where $\langle \cdot \rangle_0$ refers to contribution from just the first two

terms in Eq. (S18). Finally, we note that the second term in Eq. (S18) gives a small contribution to $\langle a^\dagger a^\dagger a a \rangle_0 / \langle a^\dagger a \rangle^2 \sim \kappa/\gamma \approx 10^{-3}$ under typical experimental conditions [45]. Therefore, we neglect this contribution when calculating $g^{(2)}(0)$.

Condensate Fraction – Figure S2 shows the condensate fraction and detuning δ_0 [defined below Eq. (18) in the main text] in one, two, and three dimensions as a function of T and N . The effective chemical potential $\mu = \hbar(\omega_c - \delta_0)$ was chosen to fix the photon density $n = 0.1$. We see that the 3D result converges to the thermodynamic limit around 10^5 resonators.

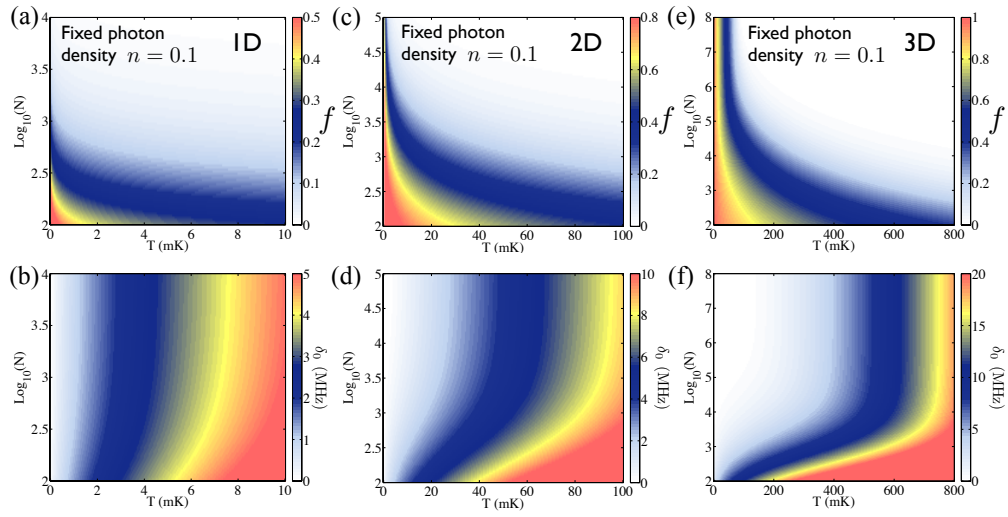


FIG. S2: Condensate fraction f and detuning δ_0 [defined below Eq. (18) in the main text] for fixed density $n = 0.1$ in 1D (a-b), 2D (c-d), and 3D (e-f) for the same parameters as Fig. 3(b) in the main text.